

4D-CT Attenuation Correction in Respiratory-Gated PET for Hypoxia Imaging: Is It Really Beneficial?

Brandon Driscoll¹, Douglass Vines^{2,3}, Tina Shek¹, Julia Publicover¹, Ivan Yeung^{1,2,3}, Stephen Breen^{2,3}, and David Jaffray^{1,2,3}

¹Quantitative Imaging for Personalized Cancer Medicine Program—Techna Institute, University Health Network, Toronto, ON, Canada; ²Radiation Medicine Program, Princess Margaret Cancer Centre, Toronto, ON, Canada; and ³Department of Radiation Oncology, University of Toronto, Toronto, ON, Canada

Corresponding Author:

Brandon Driscoll, MASC
University Health Network, Toronto M5G 2M9, Canada;
E-mail: brandon.driscoll@rmp.uhn.ca

Key Words: 4D-PET, phantom, quality assurance, hypoxia, respiratory gating

Abbreviations: positron emission tomography (PET), computed tomography (CT), attenuation correction (AC), standardized uptake values (SUV), phase-matched (PM), helical CT (hCT), fluorodeoxyglucose (FDG)

ABSTRACT

Previous literature has shown that 4D respiratory-gated positron emission tomography (PET) is beneficial for quantitative analysis and defining targets for boosting therapy. However the case for addition of a phase-matched 4D-computed tomography (CT) for attenuation correction (AC) is less clear. We seek to validate the use of 4D-CT for AC and investigate the impact of motion correction for low signal-to-background PET imaging of hypoxia using radiotracers such as FAZA and FMISO. A new insert for the Modus Medicals' QUASAR™ Programmable Respiratory Motion Phantom was developed in which a 3D-printed sphere was placed within the "lung" compartment while an additional compartment is added to simulate muscle/blood compartment required for hypoxia quantification. Experiments are performed at 4:1 or 2:1 signal-to-background ratio consistent with clinical FAZA and FMISO imaging. Motion blur was significant in terms of SUV_{max} , mean, and peak for motion ≥ 1 cm and could be significantly reduced (from 20% to 8% at 2-cm motion) for all 4D-PET-gated reconstructions. The effect of attenuation method on precision was significant (σ^2 hCT-AC = 5.5%/4.7%/2.7% vs σ^2 4D-CT-AC = 0.5%/0.6%/0.7% [max%/peak%/mean% variance]). The simulated hypoxic fraction also significantly decreased under conditions of 2-cm amplitude motion from 55% to 20% and was almost fully recovered (HF = 0.52 for phase-matched 4D-CT) using gated PET. 4D-gated PET is valuable under conditions of low radiotracer uptake found in hypoxia imaging. This work demonstrates the importance of using 4D-CT for AC when performing gated PET based on its significantly improved precision over helical CT.

INTRODUCTION

Accurate absolute quantitation of radioactivity concentration is a requirement for the use of positron emission tomography (PET) to monitor disease response. In the presence of respiratory motion, however, quantitative PET becomes challenging for 2 distinct reasons. First, the long image acquisition time required produces images that represent the average of many respiratory cycles, which introduces blurring and reduces the standardized uptake values (SUV). Second, CT scans used for attenuation correction (AC) have comparatively fast acquisition times. This produces images that represent a much shorter time frame within the respiratory cycle that can create a mismatch in breathing phases between the PET and computed tomography (CT) scans giving rise to artifacts and affect SUV values (1–23). It was hypothesized that in the presence of tissue density differences (eg, lung), the quantitation of gated PET (4D-PET) radioactivity is

improved with phase-matched (PM) gated CT (4D-CT) for AC than with AC with a standard helical CT (hCT).

However, there is a cost to gated PET, which is that by dividing the PET data into shorter time bins, the total counts left to reconstruct the image are substantially reduced, leading to increased noise in the image. Although this has minimal effect on measures such as SUV_{mean} , it can have a substantial effect on the SUV_{max} , especially in cases where the signal-to-background ratio is low. Because partial volume averaging in PET has the effect of decreasing activity in regions of higher signal and increasing activity in regions of lower signal, the difference in signal-to-background ratio will have an impact on the amount of partial volume averaging observed. For this reason, it is important to assess whether 4D-PET and 4D-CT are equally important under these low signal-to-noise ratio conditions.

Acquiring PET images of a moving target can be performed in a number of ways ranging from nongated to gated with 4D-CT PM AC. Other researchers have suggested a variety of AC methods such as using 4D maximum intensity projection (4D-MIP) of 4D-CT (4D-CT-MIP) (1, 18, 24), of PET (4D-PET-MIP) (18, 25), a fusion of the 4D-CT-MIP and 4D-PET-MIP (19), quiescent period gating (10), or the use of a time-averaged midposition 4D-CT created from applying deformable registration on all phase bins (22, 23). Scanner manufacturers have also been working toward improved 4D gating and have made reconstruction options available such as Q. Freeze on the GE (GE Healthcare, Chicago, IL) platform (phase-based gating) (24, 26, 27) and HD-Chest on the Siemens (Siemens Healthineers, Erlangen, Germany) platform (amplitude-based gating) (5, 16, 17). The methods analyzed in this study included those available on our GE Discovery 610 PET/CT system and are listed in Table 1.

A large number of papers have investigated the effects of gated PET in both phantom (1, 3–5, 18, 20, 27) and clinical situations (6–10, 12, 13, 18, 21–26, 28, 29). However, the methods of analysis differed greatly, and most of them investigated only high signal-to-background scenarios found in fluorodeoxyglucose (FDG) ($SUV \geq 5$ even in lung nodules imaging (12) while only a small minority (22, 29) mentioned hypoxia imaging with its much lower signal-to-background ratio (30–31). Although all have shown advantages of performing gated PET, the improvements from using a 4D-CT for AC have been less clear (1–4, 26), and therefore, the use of 4D-CT and its additional radiation dose to the patient needs to be justified. In the work done by Nyflot et al (1), the results of AC with 4D-CT were comparable with those of hCT, and only the MIP-CT-based AC was able to fully recover the loss of PET signal due to motion. The authors did acknowledge that this may be a result of overcorrection owing to the artificially high CT values generated by the use of MIP.

Much of the above reported work compared SUV_{max} only between methods. The SUV_{max} represents only a single voxel of an entire PET image, and as PET images are inherently noisy, SUV_{max} , although a mainstay of PET analysis, can change considerably under different reconstructions. SUV_{max} is typically used in PET, as it is not affected by variations of region of interest definition.

Many studies (1, 3, 14–15, 24) in the literature that analyze 4D-PET look at the SUV_{max} difference between the nongated and gated PET, but in many cases, the effect of additional noise in the gated PET and its impact on SUV_{max} is not mentioned. Some authors do correct for this using a shortened nongated PET image (6, 17) to do a proper comparison between SUV_{max} of gated and nongated scans. Other metrics such as SUV_{peak} (32–33) or

SUV_{mean} may better represent the actual improvements occurring when comparing nongated to gated PET. For these reasons, all 3 methods are investigated in this work to investigate which ones are most impacted by 4D motion.

Most of the work done with 4D-PET has been performed using ^{18}F -FDG which typically has higher tumor uptake (14), yielding a higher signal-to-background ratio than other radiotracers such as the hypoxia marker ^{18}F -fluoroazomycin arabinoside (FAZA-PET). Hypoxia is correlated with radioresistance and metastases, which are associated with poor outcomes (34). As such, accurate identification of hypoxic regions within tumors could allow for improvements in staging and dose escalation in these regions during treatment planning. These radiotracers offer the potential to evaluate the hypoxic status serially over time and in response to treatment in individual patients.

In this study, we evaluate phantom-simulated lung imaging with respect to the estimation of hypoxic fraction (30–31). Though previous work has validated the use of 4D-PET in high signal-to-background environments, the present study seeks to validate those conclusions and also to look at the specific case of low signal-to-background situations as seen with FAZA.

The efforts of Mortensen (30) and Muzi (31) have established the groundwork for quantitative hypoxia imaging, an additional investment in scientific investigation, international collaboration, and clinical research is required to mature these methods to the point of broad dissemination and collective learning (35). These efforts include addressing the technical challenges of PET and CT scanner calibration, developing standardized imaging protocols, accommodating physics-related artifacts (eg, scatter and partial volume effects). Towards this goal, the effects of 4D-PET on the simulated hypoxic fraction (30–31) will also be investigated. A novel phantom insert was created which incorporates not only a lung and tumor compartment, as in the work of Nyflot et al. (1), but also a third “muscle/blood” surrogate compartment to allow for the generation of the hypoxic threshold (30–31) used in calculating the hypoxic fraction.

This work aims to validate existing work relating to 4D-gated PET in terms of different SUV-based metrics (max, peak, and mean) at low signal-to-noise levels while additionally exploring the effect on hypoxic fraction quantification.

METHODS

Phantom Design

A new adaptable insert for the Modus Medicals (Modus QA, London, ON, Canada) QUASAR™ Programmable Respiratory Motion Phantom was developed for this study. This computer-

Table 1. 4D Respiratory PET Motion-Correction Options

Name	Nongated	Nongated (100)	hCT-AC	PM AC	Q. Freeze
PET	Nongated (1 Bin)	Nongated	6 Bin Gated	6 Bin Gated	6 Bin Gated (Registered)
Time Per Bin (seconds)	600	100	100	100	600 ^a
CT used for AC	Helical CT	Helical CT	Helical CT	4D-CT	4D-CT

^a Using Q. Freeze, the 6 PET bins are registered together and then averaged, resulting in a single motion-corrected 600-second noise-equivalent bin.

controlled phantom allows the simulation of arbitrary breathing patterns (including those obtained with the Varian RPM video camera-based system). The phantom is shown in Figure 1. Cylindrical inserts, within a torso-shaped acrylic shell, move in the superior/inferior direction with varying speeds and amplitudes.

We have designed, and built, a 4D-PET insert compatible with this motion platform to explore image quality issues brought on by breathing motion in 4D-PET-CT. The insert is a hollow acrylic cylinder with a removable “target” lesion. For this study, we have built a spherical target with a 30-mm inner diameter. The cylinder and target can be filled separately to allow for varying signal-to-background ratios. In addition, the insert can be filled with polystyrene beads to mimic lung density.

In the assessment of hypoxia by PET-CT with FAZA or other radiotracers such as ^{18}F MISO, typically the signal in the tumor is compared with a reference nonhypoxic surrogate such as blood or muscle to determine the level of hypoxia. To evaluate the effect of 4D-PET in this analysis, the 4D phantom insert was designed with an additional background surrogate section which would not contain the polystyrene beads and would represent the muscle or blood (Figure 1, B and C).

Experimental Setup

A moderately low signal-to-background ratio of 4:1 was evaluated for the experiments detailed in the following sections based on clinical experience with FAZA in lung tumors. An additional lower signal-to-background concentration level of 2:1 was tested when evaluating the impact of gating on hypoxic fraction.

Phantom Motion. For each setup, the phantom was imaged under conditions of no motion to generate a baseline static image with which to compare the 4D-PET results. A sinusoidal waveform with a breathing frequency of 15 BPM and amplitude was set to 0.5, 1, and 2 cm of peak-to-peak motion based on experience with patients.

Image Acquisition. All phantom scans were acquired on a GE Discovery 610 system using the clinical lung protocol consisting of:

1. Low-dose hCT for AC.
2. PET acquisition:
 - axial fields of view;
 - list mode on; and
 - respiratory gating using the Varian RPM motion tracking system.
3. 4D-CT:
 - using the Varian RPM motion tracking system.

The PET data were binned into either 1 (nongated) or 6 bins and reconstructed on the GE Discovery Console using the hCT and the MP of the 4D-CT for AC. The PET acquisitions were performed with the clinical protocol of 10 minutes and 2 bed positions.

An additional reconstruction of only the first 100 seconds of the nongated phantom image was performed as discussed by Guerra et al. (6) to ensure noise characteristics are even between the nongated and gated images.

GE Q. Freeze. GE provides an optional motion correction package for their PET-CT systems marketed as “Q. Freeze”. This software performs deformable registration on the gated PET image to 1 reference gate. The resulting registered 6 PET volumes are then averaged to provide a new PET image. This Q. Freeze PET image should then provide a motion-corrected image with minimal or reduced blurring while keeping the noise level properties of a nongated PET.

Effect of Different hCTs on the Resulting 4D-PET Images. To assess the impact of the variability of the hCT and 4D-CT acquisitions on the 4D respiratory-gated PET images, a reproducibility experiment was performed. This set of experiments was performed at 4:1 signal-to-background ratio and 2-cm amplitude where a single gated PET was obtained alongside 10 separate hCTs and 10 separate 4D-CTs. The exhale bin (36) (ie, bin 4 of 6) of the gated PET was then reconstructed using each of the 10 4D-CT exhale bins as well as from the 10 hCT s.

Image Analysis

Images were downloaded from the GE system in DICOM format and then imported into MIM (MIM software, Cleveland, OH)

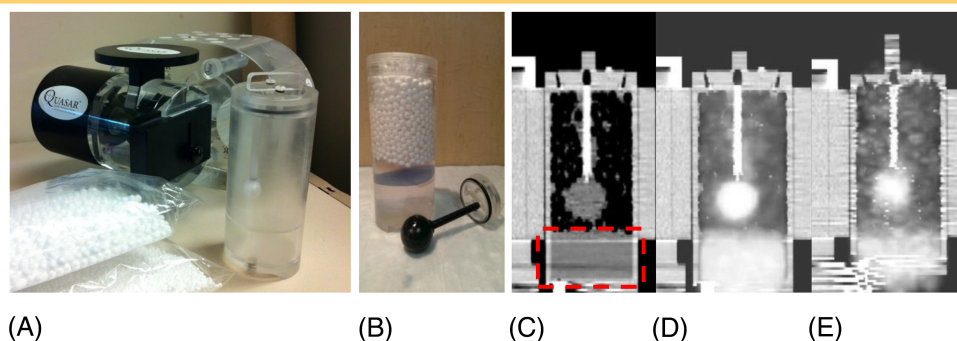


Figure 1. Custom-made 4D positron emission tomography (PET) insert for the Modus Medical QUASAR TM Programmable Phantom. (A) Modus Phantom and custom-made fillable spherical insert with a separator plate to create a third “muscle/blood” surrogate compartment (dashed rectangle in panel C). (B) Photo of 3-section insert (lung, tumor, and surrogate), (C) a corresponding computed tomography (CT) image, and (D) the fused PET-CT image of a static scan and one in motion without gating (E).

where the corresponding CT and PET were selected and registered and then sent to MATLAB (The MathWorks Inc., Natick, MA) for analysis.

A MATLAB script was run on each volume that determined the location of the center of mass (weighted based on PET activity) of the activity contained within the sphere. The weighted center of mass was then used to create a virtual 30-mm spherical region of interest at that location for analysis.

These generated spherical regions were used in each AC method to calculate the various metrics at each phase bin. Hence, a direct comparison between AC methods at each phase bin could be made. The activity measurements from the static scan were also quantitated to determine deviations from the known injected activity.

The measured radioactivity in a 1-cm ROI surrounding the highest activity region of the sphere (33) (SUV_{peak}) was determined for each phase of motion for all 4D-PET data with hCT for AC and PM 4D-CT for AC.

An additional cylindrical region was created in the background “surrogate” region for the HF and signal-to-background calculations. Sphere-to-background ratios were calculated using the sphere peak or max and surrogate section mean. The hypoxic fraction was calculated using a threshold defined as either the mean of the surrogate section plus 3 standard deviations as per Mortensen et al. (30) or the surrogate multiplied by a factor as per Muzi et al. (31)

RESULTS

Effect of Gated PET on Radioactivity Recovery in 4D-PET at Low Signal-to-Background Ratio

The results of the 4:1 signal-to-background scan with the phantom at 15 BPM and 2-cm peak-to-peak amplitude are displayed in Figure 2. The maximum pixel (Figure 2A) value is increased when compared with the static scan as a result of the images becoming noisier when binned which decreases the counts by a factor of 6 (10). To confirm this fact, an additional reconstruction was performed for each of the scenarios which used only the first 100 seconds (nongated 100 seconds) of each axial field of view of the acquisition to maintain the same noise properties as the

gated PET images (600 seconds per axial field of view for 4D-gated PET/6 bins = 100 seconds per bin).

The max of the nongated 100 seconds is increased for 0.5-, 1.0-, and 2.0-cm motion confirming that increased noise is playing a larger role than the blurring effect caused by motion. Interestingly, the GE Q. Freeze reconstruction reduces the max value in all situations as compared to the PM images as a result of the decreased noise resulting from the averaging performed across all PET bins using the method (6).

The effect of gated PET on the SUV_{peak} and mean is only subtly observed with an amplitude of 0.5 cm (2%–3%) but increases to as much as 9% at 1-cm amplitude. At 2-cm amplitude, the mean activity is decreased by 20.1% and the helical CT AC, PM AC, and Q. Freeze methods reduced the decrease to -7.2, -8.2, and -8.7% respectively. The same correction is less evident with peak where there is only weakly significant ($P < .05$) correction in the PM AC and Q. Freeze methods and none with hCT-AC ($P > .05$).

Each reconstruction approach provided a significant increase in mean PET signal as compared with nongated ($P < .01$); however, there was no significant difference between the approaches in terms of peak ($P > .05$) or mean activity ($P > .05$), as helical CT AC, PM, and Q. Freeze all provided very similar results.

Signal-to-Background Recovery

As in the previous section, the effect on the sphere-to-background ratio (designed to be 4:1) based on the maximum value is misleading (Figure 3A) as the increase in signal-to-background is purely the product of greater noise. This is abundantly clear as the signal-to-background levels are actually even higher than the ones obtained in the static case. Note: the experimental setup produced a signal-to-background ratio of 3.95:1 as measured by a well counter. However, the peak intensity of a small 3-cm sphere is still affected by partial volume effect which resulted in a sphere to background ratio of 3.6:1 based on the static sphere.

Because the effect of 4D-PET on the SUV_{peak} at 0.5 or 1 cm was <5% in the previous section, it was expected that similar

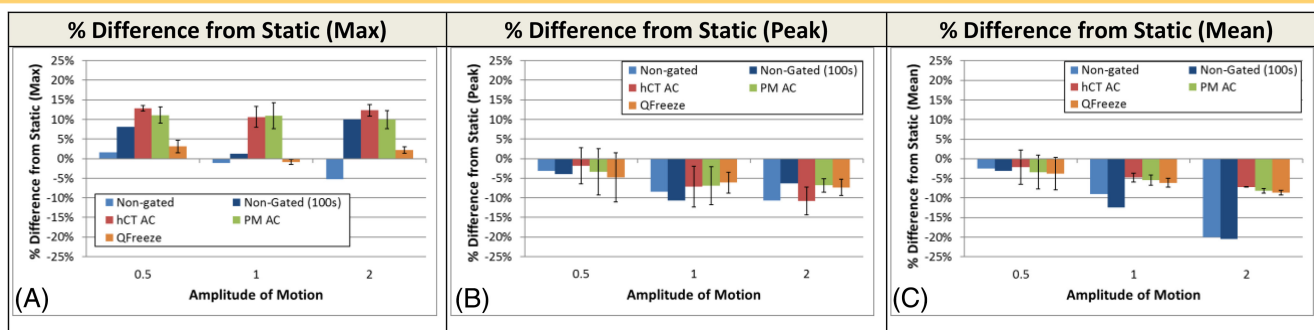


Figure 2. Effect of low signal-to-background ratio on 4D-PET results. Comparison of nongated PET (blue), helical attenuation correction (AC)-gated PET (red), phase-matched (PM) (green)-gated PET, and Q.Freeze-gated (orange) to the static scan at a motion amplitude of 2 cm analyzed by max (A), peak (B), and mean (C). Error bars on the PM- and helical AC-gated images represent the standard deviation of the 6 bins.

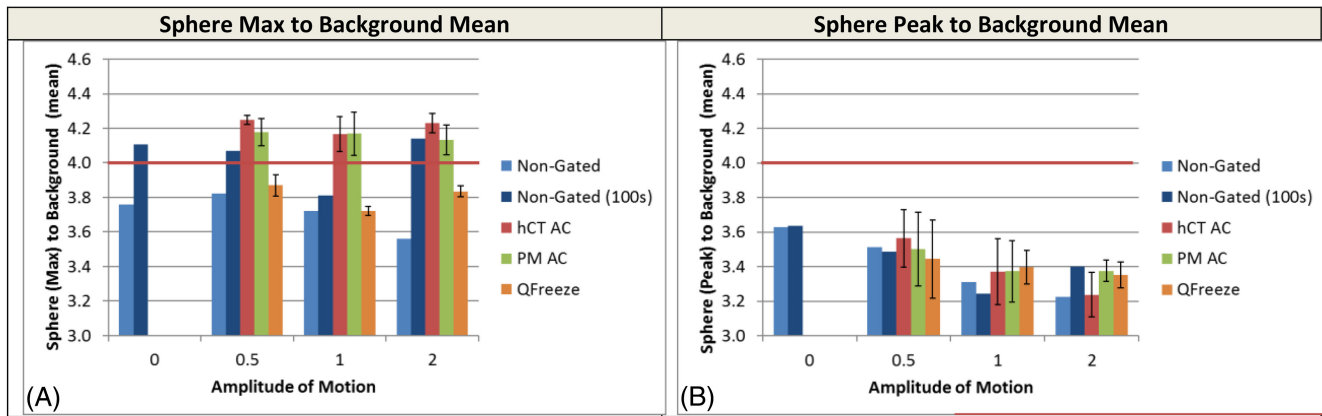


Figure 3. Effect of 4D-PET on sphere-to-background ratio. The sphere-to-background ratios of the nongated PET (blue), helical AC-gated PET (red), and PM- (green) gated PET analyzed by max (A) and peak (B) versus surrogate mean. Error bars on the PM- and helical AC-gated images represent the standard deviation of the 6 bins.

effects on the image-derived signal-to-background ratios would be observed. This was confirmed in Figure 3, as the signal-to-background ratios were reduced from 3.6 to 3.5 (3%) or 3.4 (6%) at 0.5 and 1 cm amplitude respectively.

Under conditions of 2-cm motion, the sphere (peak)-to-background ratio decreased by as much as 11% while 4D gating for PET could recover about 5% of this for PM AC and Q. Freeze. Attenuation correction with hCT could not affect a similarly significant change and resulted in sizeable variance, which will be investigated in the section entitled “Evaluating the Difference between 4D-CT and Helical CT Attenuation Correction on 4D Respiratory Gated PET.”

Effect on Hypoxic Fraction

The simulated “hypoxic fraction” of the sphere is derived from the fact that, owing to partial volume effects, not all the

parts of the sphere will have equally high intensity. As such, in the absence of partial volume effect, the sphere should have a hypoxic fraction of 1. However, partial volume averaging works as a surrogate for nonhypoxic regions in this case and as such the effect of 4D-PET and motion on hypoxia measurement can effectively be estimated (Figure 4). Because of this approach, the 4:1 signal-to-background was too high to detect differences in the reconstruction and gating technique so an even lower 2:1 signal-to-background was used for these experiments.

The hypoxic fraction can be calculated in 2 different ways. Mortensen et al. (30) rely on looking at the region of the tumor with a signal greater than a threshold of the mean activity in a nonhypoxic area (typically muscle) plus 3 times the standard deviation in the region. Thus, as the nonhypoxic area becomes noisier, the hypoxic fraction will be reduced. Muzi et al. (31) use

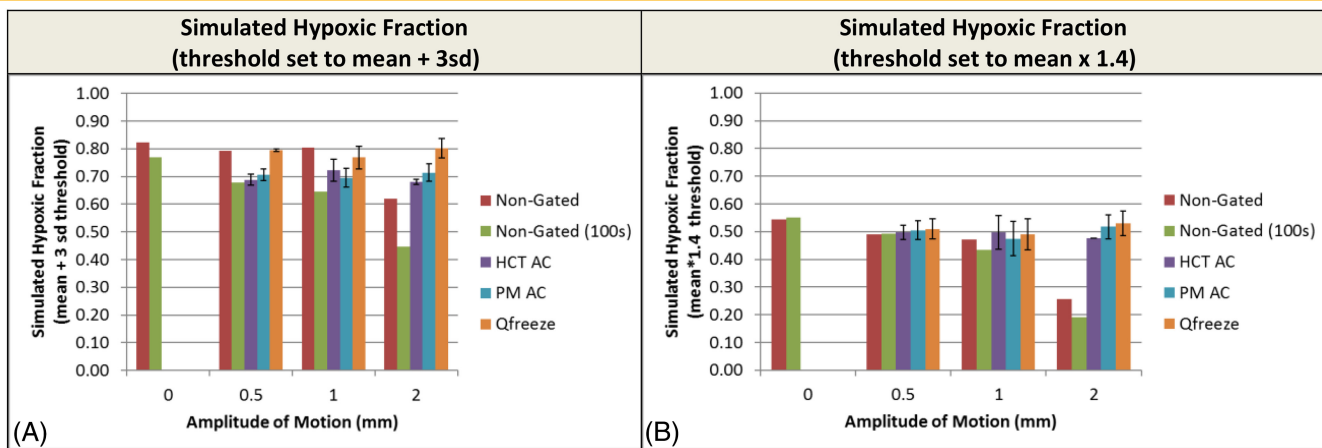


Figure 4. Effect of 4D-PET on simulated hypoxic fraction calculation. Hypoxic fraction generated by either a noise-based threshold (A) or a fixed threshold (B) is displayed for the experiment performed at a 2:1 signal-to-background ratio. Error bars on the PM and helical AC-gated images represent the standard deviation of the 6 bins.

fixed cutoff values between 1.2 and 1.4 times the surrogate (typically blood) activity to define the cutoff.

In Figure 4, the hypoxic fraction is calculated using both approaches. When using the noise-based method (15) (Figure 4A) the hypoxic fraction is reduced 5% even under static conditions when comparing the nongated and nongated 100 images, owing to the fact that as noise levels are increased, the resulting higher threshold lowers the hypoxic fraction. This same effect is not evident when using a fixed (1.4 x mean) threshold (Figure 4B).

The motion results for the noise-based hypoxic fractions (Figure 4A) are interesting but not unexpected. In all cases, the nongated (100 seconds) have a reduced hypoxic fraction owing to the combination of increased noise and motion blur (−10%, −15%, and −30% at 0.5-, 1-, and 2-cm motion). For the gated results, both hCT and 4D-CT-corrected image sets are able to recover most of the hypoxic fraction at 2-cm motion (from 0.44 to 0.68 and 0.70, respectively). Q. Freeze interestingly recovers all of the lost hypoxic fraction because of the fact that it decreases the noise, thereby decreasing the hypoxic threshold, while simultaneously decreasing motion blur. This effect is completely eliminated when the hypoxia threshold is selected based on the mean × 1.4 (Figure 4B). The plot of fixed threshold hypoxic fraction shows a lower static hypoxic fraction owing to the higher threshold using mean × 1.4; however, the same 30% reduction in hypoxic fraction at 2-cm motion is detected. In the absence of noise-based thresholds, all 3 gating/reconstruction methods are able to recover the hypoxic fraction lost because of motion blur.

Evaluating the Difference Between 4D-CT and Helical CT Attenuation Correction on 4D Respiratory-Gated PET

Because the hCT-attenuated gated PET images provided very similar results to the 4D-CT PM for all metrics investigated through the previous sections, an additional 4:1 signal-to-background experiment was performed in which 10 different hCT s and 10 different 4D-CTs were used to reconstruct with

the same gated PET data. The results of these scans are displayed in Figure 5.

As in the previous sections, both the max and peak activity show an increase in activity because of decreased bin time, while as expected, the 4D gated PET results show a substantially higher value than nongated results. Although the mean percent differences in terms of both max and peak for hCT and 4D-CT are not significantly different from each other ($P > .05$), in both cases, the precision of the 4D-CT PM reconstruction is much higher than the hCT corrected data (σ^2 hCT-AC = 5.5%/4.7%, σ^2 4D-CT-AC = 0.5%/0.6% [max%/peak% variance]). This result is also evident in the mean activity where both the helical and 4D-CT data are corrected almost back to the static scan and the helical data have a slightly higher (although nonsignificant) mean than the 4D-CT (σ^2 hCT-AC = 2.7%, σ^2 4D-CT-AC = 0.7%). This suggests that while the mean value achieved with hCT-based AC will be the same as 4D-CT, there can be a significant impact on max or peak values depending on where the hCT catches the tumor in the breathing cycle.

DISCUSSION

4D respiratory-gated PET, using any of the 3 selected methods illustrated (hCT, PM, or Q. Freeze), was effective under situations of motion >1cm in reducing or eliminating motion blur. However, there was only a limited difference between the methods of gating in terms of max, peak, or mean activity. To demonstrate the importance of performing 4D-CT-based AC, the final reproducibility experiment was performed showing that there was a dramatic increase in precision when using 4D-CT vs helical AC. Thus, depending on when the hCT is started in the breathing cycle, the quantitative results differ, whereas for 4D-CT, the quantitative results are stable.

This effect is seen solely as a result of the AC approach, as both sets of experiments used the exact same list mode PET data. The importance of the accurate CT measurement provided by 4D-CT stems from the fact that if the hCT yields density values lower than reality, the PET image will be undercorrected, leading to

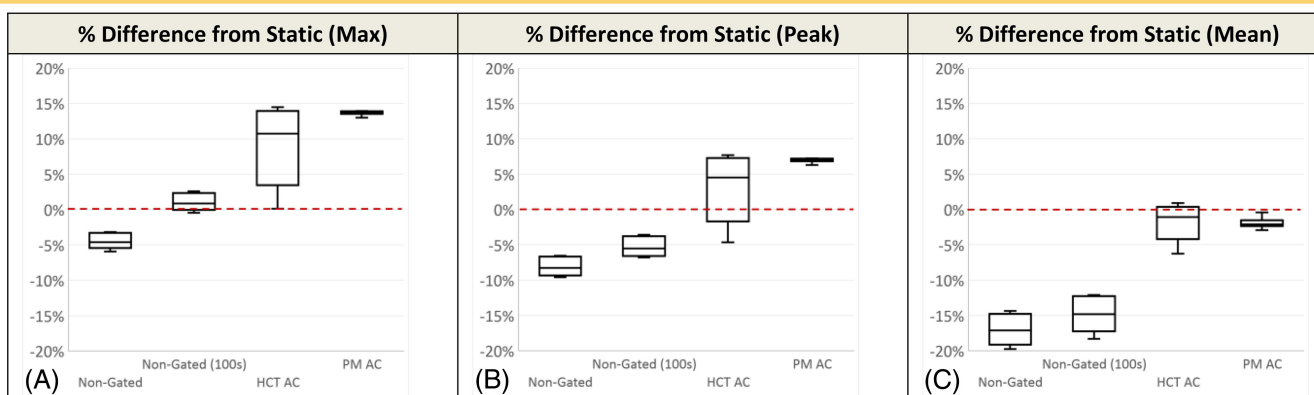


Figure 5. PM AC provides a more precise recovery of PET signal than helical AC. Box and whisker plots of max (A), peak (B), and mean (C) PET activity compared with static are displayed. Each CT scan was repeated 10 times, resulting in $n = 10$ of each PET series.

lower activity values. Conversely, higher CT density values can lead to overcorrection and higher PET values.

To confirm this fact, the CT number of a larger 6-cm spherical region of interest surrounding the actual sphere (3 cm) was plotted against the resulting radioactivity for each phase of each of the 10 sets of hCT attenuation corrected images in Figure 6. A larger sphere was required, as the density within the sphere affects not only the AC for PET but also the entire area surrounding the sphere between the signal and detector; 6 cm was selected, as it represents the size of the sphere plus the amplitude of motion where differences in the CT value will be detected.

This figure shows that there is a clear correlation ($R^2 = 0.992$ for nongated and 0.94 for helical-gated) between the CT number and radioactivity, which is not unexpected. The difference between the lowest and highest values was 13% for the same original PET data. Figure 6 also shows how hCT-corrected 4D-PET values can sometimes be higher or lower than their corresponding 4D-CT values because of either over- or undercorrection of the PET values based on the CT. The 4D-CT values show up in a cluster with very similar CT numbers (between -399 and -420 HU) and as a result generate a much more precise and consistent set of PET values than their hCT-corrected counterparts. These results are consistent with the findings of Kruis et al. (28), who found a strong correlation between average CT number and SUV_{mean} in primary lung tumors of 32 patients with lung cancer. Holman et al. (20) investigated the impact of density and motion on gated PET image reconstruction in FDG and FMISO. They also reported that lung CT density changes due to lung compression/expansion, and location mismatch, or breathing cycle changes could result in PET/AC-map mismatch, and thus significant PET quantitation errors.

One limitation of this study is that all the work was performed on a sinusoidal breathing curve, and as a result, the coregistration between the 4D-gated PET and 4D-CT was very good. It has been suggested by Nyflot et al. (1) that the errors in CT gating in clinical examples could result in errors in PET AC even when performing 4D-CT. Our work supports that hypothesis and also attempts to quantify it using the 10 separate hCTs that also simulate the effect of poor registration.

In some reported work (1, 18, 24) an MIP from a 4D-CT was used to perform the AC. We argue that this will generally overcorrect the PET value, as the CT values will be higher owing to the nature of an MIP, and Figure 6 supports this fact. However, the GE system used in these experiments did not have the ability to reconstruct from an MIP CT image to prove this conclusively. Caution should be taken using CT-MIPs when breathing patterns are irregular in amplitude or periodicity (37), and Callahan et al. (18) suggest these may not help under conditions of poor soft tissue contrast (eg, tumors neighboring other soft tissues, heterogeneous tumors, etc.).

Much of the reported literature (1, 14, 15, 24) in the area of 4D-PET compares only SUV_{max} values between different methods, while many other works (6, 11, 12) use the “Best Bin” to determine which method has the higher recovery of signal. This method of analysis performed as the SUV_{max} is less sensitive than the effects of region of interest selection and partial volume averaging. Despite these arguments in their favor, this approach must be performed using a great deal of caution, especially for studies with limited signal-to-background ratios and high noise levels (eg, images using FMISO, FAZA, etc.). By displaying the nongated PET results using both a 600-second and 100-second PET-CT in Figures 2 and 3, it is clear that by decreasing the scan duration, the max value will increase purely because of the noise.

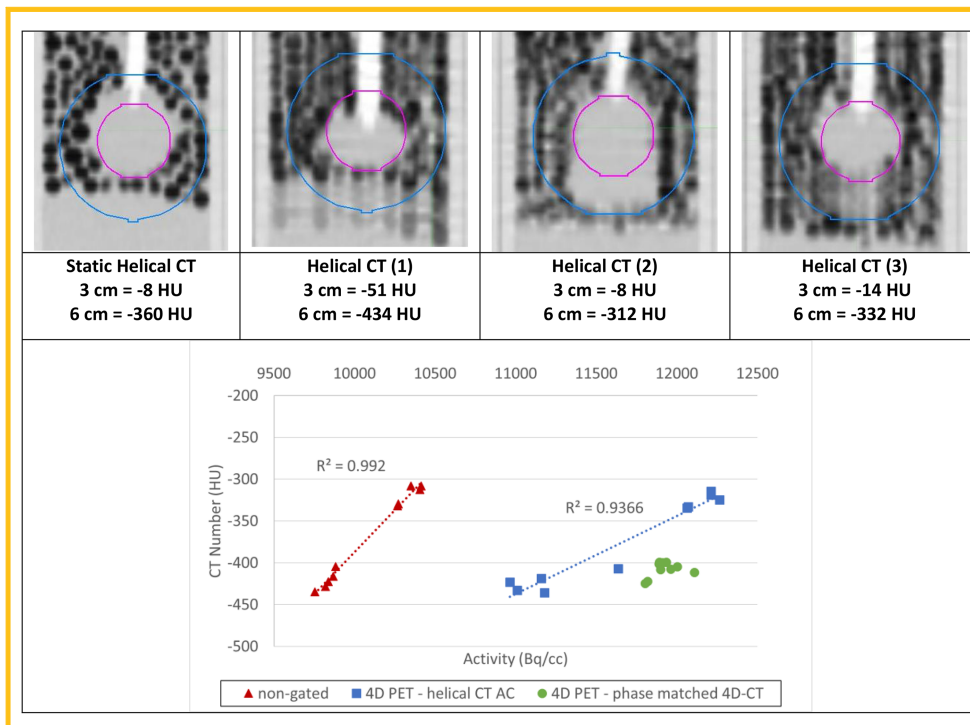


Figure 6. Depending on where the helical CT (hCT) catches the sphere in the breathing pattern (top), there is a clear correlation ($R^2 = 0.99$ for nongated, $R^2 = 0.94$ for helical gated) between mean sphere radioactivity (kBq) and CT number (HU) (bottom) for the 10 different hCTs used to generate the nongated and gated hCT-AC-based PET acquisitions. The 4D-CT numbers remain clustered and produce similarly clustered pet activity values.

If solely using the max for comparison, it is imperative that the same noise level be kept consistent when comparing results (ie, nongated 100 seconds to PM AC-gated).

In a small-scale study by Watanabe et al. (29) comparing nongated to gated FMISO-PET images of 5 patients with non-small cell lung cancer, it was reported that hypoxic volumes and other hypoxia quantitative metrics were significantly higher after gating. Unlike the present study, their group quantified hypoxia-based only on SUV_{mean} values of the tumor and reference muscle (and venous blood was sampled and cross-calibrated, not imaged). Nevertheless, they stated that applying 4D-PET gating is necessary to avoid underestimating tumor hypoxia from nongated PET scans.

The Q. Freeze software provided a means to generate a single motion-corrected PET while maintaining the noise levels from the nongated PET image. This approach was relatively efficient and only took a few minutes to run for each scan. As shown by others (26–27), Q. Freeze had the effect of reducing the SUV_{max} in many cases but as discussed this does not mean it was as ineffective relative to other metrics such as SUV_{mean} and SUV_{peak} , which were corrected to the same degree as the PM AC-gated images. This suggests that Q. Freeze (and comparable motion correction algorithms provided by other manufacturers (5, 16, 17)

may be useful when calculating a metric such as hypoxic fraction using the Mortensen method (30), which relies on image noise levels to provide quantitative results.

CONCLUSION

It has been widely accepted that 4D gating of PET data is a vital means of creating accurate 4D-PET images for studies with significant respiratory motion (albeit with increased noise). What has been less clear was whether 4D-CT was a valuable addition to this approach if the mean PET activity was not significantly increased. The results of this work confirm those of other literature of the benefits of PET gating using PM AC 4D-CT and also provides a detailed explanation of why 4D-CT is beneficial in the clinic to avoid high variability in PET SUV when there is motion above 1 cm. This work also investigated the effect of 4D gating at low signal-to-background scenarios as observed with low-avidity radiopharmaceuticals. Volume measurements with low activity are susceptible to stochastic noise when images are acquired for short times, which can also affect quantitative hypoxia values. It is recommended to use fixed hypoxia thresholds in these scenarios, or apply reconstruction methods such as Q. Freeze that use image averaging to reduce PET noise.

ACKNOWLEDGMENTS

This work was funded in part by grant from the Ontario Research Fund (ORF_RE_04-026), which was matched in part with contributions from General Electric Scientific. Additional funding was provided to the QIPCM Imaging Core Lab by the Ontario Institute for Cancer Research and Princess Margaret Cancer Centre Foundation. The work was also partly supported by the Quantitative Imaging Network grant funded by the Canadian Institute of Health Research.

Conflict of Interest: None reported.

Disclosures: No disclosures to report.

REFERENCES

- Nyflot MJ, Lee T-C, Alessio AM, Wollenweber SD, Stearns CW, Bowen SR, Kinahan PE. Impact of CT attenuation correction method on quantitative respiratory-correlated (4D) PET/CT imaging. *Med Phys*. 2014;42:110–120.
- Huang TC, Chou KT, Wang YC, Zhang G. Motion freeze for respiration motion correction in PET/CT: a preliminary investigation with lung cancer patient data. *Biomed Res Int*. 2014;2014:167491. [Epub 2014 Aug 28]
- Wollenweber SD, Gopalakrishnan G, Thielemans K, Manjeshwar RM. Evaluation of the accuracy and robustness of a motion correction algorithm for PET using a novel phantom approach. *IEEE Trans Nucl Sci*. 2012;59:123–130.
- Nehme SA, Erdi YE, Ling CC, Rosenzweig KE, Squire OD, Braban LE, Ford E, Sidhu K, Mageras GS, Larson SM, Humm JL. Effect of respiratory gating on reducing lung motion artifacts in PET imaging of lung cancer. *Med Phys*. 2002;29:366–371.
- Vines DC, Keller H, Hoisak JDP, Breen SL. Quantitative PET comparing gated with nongated acquisitions using a NEMA phantom with respiratory-simulated motion. *J Nucl Med Technol*. 2007;35:246–251.
- Guerra L, De Ponti E, Elisei F, Bettinardi V, Landoni C, Picchio M, Gilardi MC, Versari A, Fioroni F, Dziuk M, Koza M, Ahond-Vionnet R, Collin B, Messa C. Respiratory gated PET/CT in a European multicenter retrospective study: added diagnostic value in detection and characterization of lung lesions. *Eur J Nucl Med Mol Imaging*. 2012;39:1381–1390.
- Pépin A, Daouk J, Bailly P, Hapley S, Meyer ME. Management of respiratory motion in PET/computed tomography: the state of the art. *Nucl Med Commun*. 2014;35:113–122.
- Bettinardi V, Picchio M, Di Muzio N, Gilardi MC. Motion management in positron emission tomography/computed tomography for radiation treatment planning. *Semin Nucl Med*. 2012;42:289–307.
- Killoran JH, Gerbaudo VH, Mamede M, Ionascu D, Park SJ, Berbeco R. Motion artifacts occurring at the lung/diaphragm interface using 4D-CT attenuation correction of 4D PET scans. *J Appl Clin Med Phys*. 2011;12:3502.
- Liu C, Alessio A, Pierce L, Thielemans K, Wollenweber S, Ganin A, Kinahan P. Quiescent period respiratory gating for PET/CT. *Med Phys*. 2010;37:5037–5043.
- García Vicente AM, Castrejón AS, León Martín AA, García BG, Pilkington Woll JP, Muñoz AP. Value of 4-dimensional 18F-FDG PET/CT in the classification of pulmonary lesions. *J Nucl Med Technol*. 2011;39:91–99.
- Guerra L, Meregalli S, Zorz A, Niespolo R, De Ponti E, Elisei F, Morzenti S, Brenna S, Crespi A, Gardani G, Messa C. Comparative evaluation of CT-based and respiratory-gated PET/CT-based planning target volume (PTV) in the definition of radiation treatment planning in lung cancer: preliminary results. *Eur J Nucl Med Mol Imaging*. 2014;41:702–710.
- Tahari AK, Lodge MA, Wahl RL. Respiratory-gated PET/CT versus delayed images for the quantitative evaluation of lower pulmonary and hepatic lesions. *J Med Imaging Radiat Oncol*. 2014;58:277–282.
- Sindoni A, Minutoli F, Pontoriero A, Iati G, Baldari S, Pergolizzi S. Usefulness of four dimensional (4D) PET/CT imaging in the evaluation of thoracic lesions and in radiotherapy planning: review of the literature. *Lung Cancer*. 2016;96:78–86.
- Frood R, McDermott G, Scarsbrook A. Respiratory-gated PET/CT for pulmonary lesion characterisation—promises and problems. *Br J Radiol*. 2018;91:20170640.
- Gillman A, Smith J, Thomas P, Rose S, Dowson N. PET motion correction in context of integrated PET/MR: current techniques, limitations, and future projections. *Med Phys*. 2017;44:e430–e445.
- Grootjans W, de Geus-Oei LF, Meeuwis AP, van der Vos CS, Gotthardt M, Oyen WJ, Visser EP. Amplitude-based optimal respiratory gating in positron emission tomography in patients with primary lung cancer. *Eur Radiol*. 2014;24:3242–3250.
- Callahan J, Kron T, Schneider-Kolsky M, Dunn L, Thompson M, Siva S, Aarons Y, Binns D, Hicks RJ. Validation of a 4D-PET maximum intensity projection for delineation of an internal target volume. *Int J Radiat Oncol Biol Phys*. 2013;86:749–754.

19. Callahan J, Kron T, Siva S, Simoens N, Edgar A, Everitt S, Schneider ME, Hicks RJ. Geographic miss of lung tumours due to respiratory motion: a comparison of 3D vs 4D PET/CT defined target volumes. *Radiat Oncol*. 2014;9:291.
20. Holman BF, Cuplov V, Hutton BF, Groves AM, Thielemans K. The effect of respiratory induced density variations on non-TOF PET quantitation in the lung. *Phys Med Biol*. 2016;61:3148.
21. Thomas HM, Kinahan PE, Samuel JJE, Bowen SR. Impact of tumour motion compensation and delineation methods on FDG PET-based dose painting plan quality for NSCLC radiation therapy. *J Med Imaging Radiat Oncol*. 2018;62:81–90.
22. Di Perri D, Lee JA, Bol A, Hanin FX, Janssens G, Labar D, Robert A, Sterpin E, Geets X. Correlation analysis of [18F] fluorodeoxyglucose and [18F] fluoroozomycin arabinoside uptake distributions in lung tumours during radiation therapy. *Acta Oncologica*. 2017;56:1181–1188.
23. Wolthaus JW, Sonke JJ, van Herk M, Damen EM. Reconstruction of a time-averaged midposition CT scan for radiotherapy planning of lung cancer patients using deformable registration. *Med Phys*. 2008;35:3998–4011.
24. van Elmpit W, Hamill J, Jones J, De Ruyscher D, Lambin P, Öllers M. Optimal gating compared to 3D and 4D PET reconstruction for characterization of lung tumours. *Eur J Nucl Med Mol Imaging*. 2011;38:843–855.
25. Lamb JM, Robinson C, Bradley J, Laforest R, Dehdashti F, White BM, Wuenschel S, Low DA. Generating lung tumor internal target volumes from 4D-PET maximum intensity projections. *Med Phys*. 2011;38:5732–5737.
26. Minamimoto R, Mitumoto T, Miyata Y, Sunaoka F, Morooka M, Okasaki M, Igaru A, Kubota K. Evaluation of a new motion correction algorithm in PET/CT: combining the entire acquired PET data to create a single three-dimensional motion-corrected PET/CT image. *Nucl Med Commun*. 2016;37:162–170.
27. Havariyoun G, Ruiz D, Kalogianni E, Corcoran B, Mulholland N, Vivian G. Q. Freeze software for respiratory motion correction in PET/CT: a preliminary investigation with a respiratory motion phantom. *Eur J Nucl Med Mol Imaging*. 2015;42.
28. Kruis MF, van de Kamer JB, Vogel W V, Belderbos JS, Sonke JJ, van Herk M. Clinical evaluation of respiration-induced attenuation uncertainties in pulmonary 3D PET/CT. *EJNMMI Phys*. 2015;2:4.
29. Watanabe S, Hirata K, Okamoto S, Tamaki N. Impact of respiratory-gated FMISO-PET/CT for the quantitative evaluation of hypoxia in non-small cell lung cancer. *Perspectives on Nuclear Medicine for Molecular Diagnosis and Integrated Therapy*. Springer, Tokyo. 2016:319-326.
30. Mortensen L S, Johansen J, Kallehauge J, Primdahl H, Busk M, Lassen P, Alsner J, Sørensen B S, Toustrup K, Jakobsen S, Petersen J, Petersen H, Theil J, Nordmark M, Overgaard J. FAZA PET/CT hypoxia imaging in patients with squamous cell carcinoma of head and neck treated with radiotherapy: results from the DAHANCA 24 trial. *Radiother Oncol*. 2012;105:14–20.
31. Muzi M, Peterson LM, O'Sullivan JN, Fink JR, Rajendran JG, McLaughlin LJ, Muzi JP, Mankoff DA, Krohn KA. 18F-fluoromisonidazole quantification of hypoxia in human cancer patients using image-derived blood surrogate tissue reference regions. *J Nucl Med*. 2015;56:1223–1228.
32. Akamatsu G, Ikari Y, Nishida H, Nishio T, Ohnishi A, Maebatake A, Sasaki M, Senda M. Influence of statistical fluctuation on reproducibility and accuracy of SUV_{max} and SUV_{peak} : a phantom study. *J Nucl Med Technol*. 2015;43:222–226.
33. Wahl RL, Jacene H, Kasamon Y, Lodge MA. From RECIST to PERCIST: evolving considerations for PET response criteria in solid tumors. *J Nucl Med*. 2009;50:1225–150S.
34. MacManus M, Everitt S, Schimek-Jasch T, Li XA, Nestle U, Kong FS. Anatomic, functional and molecular imaging in lung cancer precision radiation therapy: treatment response assessment and radiation therapy personalization. *Transl Lung Cancer Res*. 2017;6:670.
35. Clarke LP, Croft BS, Nordstrom R, Zhang H, Kelloff G, Tatum J. Quantitative imaging for evaluation of response to cancer therapy. *Transl Oncol*. 2009;2:195–197.
36. Lee TC, Bowen SR, James SS, Sandison GA, Kinahan P E, Nyflot M J. Accuracy comparison of 4D computed tomography (4D-CT) and 4D cone beam computed tomography (4DCBCT). *Int J Med Phys Clin Eng Radiat Oncol*. 2017;06:323.
37. Park K, Huang L, Gagne H, Papiez L. Do maximum intensity projection images truly capture Tumor motion? *Int J Radiat Oncol Biol Phys*. 2009;73:618–625.